Food Chemistry: X 25 (2025) 102180

Contents lists available at ScienceDirect

Food Chemistry: X

journal homepage: www.sciencedirect.com/journal/food-chemistry-x

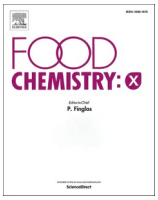

Prebiotic property of tamarind seed kernel on *Bifidobacterium animalis* growth and biofilm formation

Roongrawee Wandee [a,b], Khaetthareeya Sutthanut [a,b,*], Jenjira Songsri [a,b], Natthida Weerapreeyakul [a,b], Theera Rittirod [c], Patcharaporn Tippayawat [d], Orawan Yangkruea [a], Sirapop Jakcharoenpornchai [a]

[a] Department of Pharmaceutical Chemistry, Faculty of Pharmaceutical Sciences, Khon Kaen University, Khon Kaen 40002, Thailand
[b] Human High Performance & Health Promotion Research Institute: HHP&HP Research Institute, Khon Kaen University, Khon Kaen 40002, Thailand
[c] Department of Pharmaceutical Technology, Faculty of Pharmaceutical Sciences, Khon Kaen University, Khon Kaen 40002, Thailand
[d] Faculty of Associated Medical Sciences, Khon Kaen University, Khon Kaen, Thailand

ARTICLE INFO

Keywords:
Bifidobacterium animalis
Biofilm formation
Bioproduct
Prebiotics
Seed kernel
Tamarindus indica

ABSTRACT

This research explored the prebiotic potential of tamarind seed kernel powder (RTS), focusing on yield, nutritional composition, physicochemical properties using ATR-FTIR spectroscopy and colorimetric methods, effects on *Bifidobacterium animalis* in promoting the growth and biofilm formation compared to inulin using bacterial enumeration and crystal violet staining techniques, and the biofilm biomolecular composition characterization. The multi-nutrient composition RTS yielded 65.65 % (*w/w*), which significantly exhibited prebiotic activity in a dose-dependent manner with effective concentrations at 2.5 and 5 % RTS, stimulated *B. animalis* growth (rate 22 % • h^{-1}) and enhanced biofilm formation (BFI = 256.71) exceeding the inulin. Moreover, ATR-FTIR spectroscopy and PCA analysis revealed the RTS-induced alteration of the biofilm's biomolecular composition, with a notable increase in amide A and a decrease in carboxylic hydroxyl groups. The study highlights RTS as a promising prebiotic agent with the potential for improving gut health, with further validation in the *in vivo* models being advisable.

1. Introduction

Tamarindus indica L., commonly known as tamarind, is a notable plant in Thai cuisine and traditional medicine, used for its therapeutic properties to treat ailments like colds and stomach disorders (Hamuel, 2007). Recent research has begun to uncover the potential of tamarind seeds, a byproduct with underexplored value. The seed coat is rich in catechins, offering antioxidation and antimicrobial benefits (Wandee et al., 2022). Meanwhile, the seed kernel, traditionally used as a snack, contains xyloglucan and pectin, providing industrially valuable gelling and stabilizing properties (Kaewkumsan & Hongsawadee, 2014). Despite its nutritional richness, including essential minerals and proteins, and high safety for consumption (Kumar & Bhattacharya, 2008; Yamatoya, Tabuchi, Suzuki, & Yamada, 2020), there is limited scientific evidence supporting its health benefits, particularly as a prebiotic. Therefore, advancing research in this area could reveal significant health-promoting properties, paving the way for enhanced dietary applications and economic sustainability.

Probiotics, particularly the genera Lactobacillus and Bifidobacterium, are acclaimed for their beneficial impact on human health, notably in preventing and treating gastrointestinal issues and dysbiosis. They achieve this through mechanisms like strengthening intestinal barriers, boosting immune responses, synthesizing essential nutrients, and reducing pathogenic populations (Day, Harper, Woods, Davies, & Heaney, 2019; Martens et al., 2018; Nouvenne et al., 2018; Sharma & Riva, 2020). Bifidobacteria are particularly valuable as they naturally inhabit the human gut, contributing significantly to health by balancing gut flora, enhancing immunity, reducing inflammation, and inhibiting pathogens (Lugli et al., 2019). They are primarily found in the large intestine of healthy breastfed newborns, however, their prevalence declines with age (Arboleya, Watkins, Stanton, & Ross, 2016). Consequently, *Bifidobacterium animalis*, a widely used probiotic, has gained prominence in the food industry for its health-promoting properties.

Prebiotics, functional foods that foster a balanced gut microbiota,

* Corresponding author at: Department of Pharmaceutical Chemistry, Faculty of Pharmaceutical Sciences, Khon Kaen University, Khon Kaen 40002, Thailand
E-mail address: khaesu@kku.ac.th (K. Sutthanut).

https://doi.org/10.1016/j.fochx.2025.102180
Received 22 November 2024; Received in revised form 7 January 2025; Accepted 12 January 2025
Available online 18 January 2025

include carbohydrates, proteins, and bioactive substances that serve as nourishment for probiotics and beneficial gut microflora. This leads to the production of biochemical metabolites, such as short-chain fatty acids and bacteriocins, enhancing probiotic activity and diversity (Hurtado-Romero, Del Toro-Barbosa, Garcia-Amezquita, & García-Cayuela, 2020). Prebiotics also play a critical role in promoting extracellular polymeric substance production for biofilm formation by probiotics. A biofilm of probiotic bacteria is a structured community formed by beneficial microorganisms that adhere to surfaces and produce a self-generated extracellular matrix composed of polysaccharides, proteins, and nucleic acids (Davey Mary & O'Toole George, 2000). Thus, the ability of prebiotics to enhance biofilm formation serves as a mechanism that contributes to their functional potential and efficacy, which can be examined using *in vitro* models and validated by analyzing biomolecular compositions through methods such as infrared spectroscopy (Gieroba et al., 2020; Liu et al., 2021).

The growing interest in functional foods derived from natural sources has underscored the importance of vegetables and fruits as rich sources of prebiotic agents. Despite this, only a limited number of foods, including cereals, watermelon, honeydew, papaya, rice bran, and lactulose derivatives, have been evidenced for their prebiotic properties linked to dietary fiber and nutritional content. Among these, inulin stands out as a well-known prebiotic dietary fiber present in foods such as bananas, wheat, oats, garlic, and onions (Koruri, Banerjee, Chowdhury, & Bhattacharya, 2014). However, a significant gap remains in understanding the role of these foods in probiotic biofilm formation. Grape seed flour stands out as the only one of the few studied examples, demonstrating its potential to enhance Bifidobacterial biofilm formation, which underscores a critical mechanism of prebiotic functionality (Liu et al., 2021). This highlights the importance of a more in-depth investigation into the prebiotic properties of different agricultural and edible products, including tamarind seed kernel. This investigation is crucial for enhancing the rational application and economic sustainability of these foods.

This research focused on exploring the potential of the tamarind seed kernel, with an emphasis on its prebiotic attributes. Key aspects examined include its phytochemical and nutritional profiles, water absorption and swelling capacity, and its ability to promote the growth and biofilm formation of *Bifidobacterium animalis*. Additionally, alterations in its biomolecular composition were studied. The scientific insights gained from this research are crucial for demonstrating the benefits of utilizing the tamarind seed kernel as a valuable prebiotic ingredient. This could significantly enhance its application in the development of new functional food products, adding economic value and promoting health benefits.

2. Materials and methods

2.1. Material and equipment

Aluminum chloride ($AlCl_3$), ascorbic acid, bovine serum albumin (BSA), Bradford reagent, catechin, crystal violet, D-glucose, diethyl ether, ethyl alcohol, Folin-Ciocalteu reagent, hydrochloric acid (HCl), n-hexane, phenol solution, potassium iodide-iodine reagent, quercetin, sodium carbonate, sodium chloride, sulfuric acid, 1,1-diphenyl-2-picrylhydrazyl (DPPH), 3,5-nitrosalicylic acid (DNS) were purchase from Sigma® (St. Louis, MO, USA). Rice flour and water-soluble inulin powder (food grade) were purchased from Myskinrecipe® (Bangkok, Thailand). Bifidobacterium Agar and Bifidobacterium Broth from HI-MEDIA® (Mumbai, India). *Bifidobacterium animalis* subsp.animalis TISTR 2194 was obtained from the Department of Medical Sciences, Ministry of Public Health, Thailand. All other analytical-grade chemicals were purchased from Ajax Finechem® (Auckland, New Zealand). Tamarind seeds of ripe tamarind fruits were purchased from Khon Kaen and Phetchabun Province markets.

ATR-FTIR (4500 Series, Agilent Technologies, CA, USA), Microplate reader (VarioskanTM Flash Multimode Reader, Thermo Scientific®, MA, USA), a UV spectrophotometer (UV-1700, Shimazu, Japan), a centrifugation machine (Kubota, Tokyo, Japan), a hot air oven (France Etuves, France), Whatman paper No.1 (N-1000, Tokyo Rikakikai Co. Ltd., Japan).

2.2. Preparation of tamarind seed kernel powder

Tamarind seeds (*Tamarindus indica* L.) were washed with distilled water, dried at room temperature, roasted by heat, and soaked in distilled water for 24 h to separate the kernel from the seed coat residue. The separated tamarind seed kernel was soaked in water for another 12 h, ground into powder using a blender (Panasonic®, MX-AC400), dried at 70 °C for 12 h, and kept at −20 °C for further experiment. The %yield of tamarind seed kernel powder (RTS) compared to tamarind seed kernel weight was calculated, % yield = (weight of tamarind seed kernel x 100) / weight of tamarind seed.

2.3. Water absorption and swelling ability

A modified method from Anderson, Conway, and Peplinski (1970) was applied to determine RTS's water absorption and swelling. A mixture of exactly 0.5 g of RTS (dry powder) and 5 mL distilled water was constituted in a pre-weighed 10-mL graduated cylinder to record the origin sediment volume (V1). After 24-h standing at room temperature, the volume of swelling sediment (V2) was recorded. Then, the supernatant liquid was decanted to weigh the remaining RTS sediment and used for water absorption index (WAI) and swelling index (SI) calculation, WAI = Weight of sediment (g)/ Weight of dry powder (g) and SI = (V2 - V1)/V1 was calculated following equation.

2.4. Determination of phytochemical composition

2.4.1. Determination of total phenolic content using a Folin-Ciocalteu method

The total phenolic content of RTS was determined using the Folin-Ciocalteu method (Wandee et al., 2022). The reaction mixture was constituted comprised of 50 μL of sample solution (various concentrations of standard catechin solutions or 250 μg/mL RTS solution), 25 μL of 50 % *v*/v Folin-Ciocalteu reagent, and 125 μL of 20 % *w/v* sodium carbonate, following with a 40-min incubation. Then, absorbance at 700 nm wavelength was measured using a spectrophotometer. Then, the linear calibration curve of catechin—a reference phenolic compound was established, plotting between concentrations (0–100 μg/mL) and their corresponding absorbencies. The total phenolic content was calculated and presented as mg catechin equivalence/g of RTS. Total phenolic content = $(Abs_{sample} - Abs_{blank}) / Slope \times Amount_{sample}$ (g), Abs_{sample} is the absorbance of sample solution, Abs_{blank} is the absorbance of blank, Slope is the "a" derived from the linear equation (y = ax) of the catechin calibration curve, and $Amount_{sample}$ is the amount of sample (g).

2.4.2. Determination of total flavonoid content using an aluminum chloride colorimetric assay

The total flavonoid content in the RTS was determined using a method from Wandee et al. (2022). A reaction mixture comprising of sample solution (various concentrations of quercetin solutions or 500 μg/mL RTS solution) and 5 % $AlCl_3$ solution in a 1:1 *v*/v ratio was constituted and incubated at room temperature for 30 min. Then, absorbance at 437 nm wavelength was measured using a spectrophotometer. The linear calibration curve of quercetin—a reference flavonoid compound was established, plotting between concentrations and their corresponding absorbencies. Total flavonoid content was calculated following eq. (5) and presented as mg of quercetin equivalence/g of RTS. Total flavonoid content = $(Abs_{sample} - Abs_{blank}) / (Slope \times Amount_{sample}$ (g)), Abs_{sample} is the absorbance of sample solution, Abs

$_{blank}$ is the absorbance of blank, Slope is the "a" derived from the linear equation (y = ax) of the quercetin calibration curve, and Amount $_{sample}$ is the amount of sample (g).

2.4.3. Determination of antioxidant activity using a DPPH assay

The antioxidant activity of RTS was evaluated according to the DPPH (1,1-diphenyl-2-picrylhydrazyl) scavenging method (Wandee et al., 2022) compared to ascorbic acid (vitamin C), a reference standard antioxidant. Working solutions of the samples (RTS or ascorbic acid) were separately prepared in methanol to achieve an optimal final concentration range and used for a reaction mixture constitution in a 96-well plate, comprised of a 1:1 *v*/v ratio of each sample solution and 0.2 mM DPPH. Then, the solution was incubated at room temperature for 15 min and measured the optical absorbance at 520 nm using a spectrophotometer. The percentage of inhibition can be calculated using the formula %inhibition = (Abs control − Abs sample) × 100 / Abs control, where Abs control refers to the absorbance of the methanolic DPPH solution, while Abs sample represents the absorbance of the RTS powder (or standard compounds) treated group. Next, the 50 % oxidative inhibitory concentration (IC_{50}) value for each sample was determined by extrapolating from the linear relationship between concentrations (x-axis) and corresponding % inhibition (y-axis).

2.5. Determination of nutrition

2.5.1. Characterization of nutrition composition profile using attenuated total reflection-fourier transforms infrared spectroscopy (ATR-FTIR)

The RTS powder was directly applied to a crystal window and firmly compressed by a top-fixing clamp. Afterward, ATR-FTIR (4500 Series, Agilent Technologies, CA, USA) was used to record the spectra in triplications within the wave number range of 500–4000 cm^{-1}. The reference-assigned nutrition peaks published by Mehrotra (2006), Kizil, Irudayaraj, and Seetharaman (2002), Deeyai, Suphantharika, Wongsagonsup, and Dangtip (2013), Kong and Yu (2007), and Szymanska-Chargot and Zdunek (2013) as summarized in the supplementary table (**Table S1**) were used to analyze the FTIR spectra.

2.5.2. Determination of total sugar content using a phenol-sulfuric method

The total sugar content of RTS was determined using a modified phenol-sulfuric method of Ogura, Sugiyama, Tai, Mano, and Matsuzawa (2023). Working solutions of the samples (or reference standard D-glucose) were separately prepared in distilled water to achieve an optimal final concentration range and used for a reaction mixture constitution in a 96-well plate and incubated at 80 °C for 30 min. After cooling down, optical absorbance was measured at 492 nm wavelength using a spectrophotometer. The total sugar content of RTS was calculated and presented as a percentage of total sugar in RTS. The formula for %Total sugar is as follows: %Total sugar = [(Abs sample − Abs blank) × 100] / (Slope × Amount sample (mg) x 1000), where Abs sample is the absorbance of the sample solution, Abs blank is the absorbance of the blank, Slope is the "a" derived from the linear equation (y = ax) of the D-glucose calibration curve displayed between concentrations and corresponding absorbencies, and Amount sample is the quantity of the sample (mg).

2.5.3. Determination of reducing sugar content using a dinitrosalicylic acid method

Using a modified method of Wood et al. (2012), working aqueous solutions of the samples (or reference standard D-glucose) were separately prepared to achieve an optimal final concentration range and used for a reaction mixture comprising sample solution and 1 % *w/v* dinitrosalicylic acid solution in a 1:1 *v*/v ratio in a 96-well plate and incubated in a water bath at 98 °C for 10 min. After cooling down, optical absorbance was measured at 540 nm wavelength using a spectrophotometer. The reducing sugar content of RTS was calculated and presented as % reducing sugar of RTS. %Reducing sugar = [(Abs $_{sample}$ − Abs $_{blank}$) × 100] / (Slope × Amount $_{sample}$ (mg) x 1000), in which Abs $_{sample}$ is the absorbance of sample solution, Abs $_{blank}$ is the absorbance of blank, Slope is the "a" derived from the linear equation (y = ax) of the D-glucose calibration curve plotted between concentrations and corresponding absorbencies, and Amount $_{sample}$ is the amount of sample (mg).

2.5.4. Determination of non-reducing sugar content

Non-reducing sugar content in the RTS powder was obtained from a calculation: Non-reducing sugar = Total sugar content – Reducing sugar content.

2.5.5. Determination of protein content using a modified Bradford assay

Using a modified method of Sherovski, Stojković, and Ristovska (2018), aqueous solutions of RTS powder and bovine serum albumin (BSA), a reference protein, were separately prepared and used to constitute a reaction mixture in a 96-well plate comprising sample solution and Bradford reagent followed with 5-min incubation at room temperature. Absorbance at 595 nm wavelength was measured using a spectrophotometer. The protein content was calculated and presented as a percentage of protein in RTS. %Protein = [(Abs $_{sample}$ − Abs $_{blank}$ − b) × 100] / (Slope × Amount $_{sample}$ (mg) x 1000), in which Abs $_{sample}$ is the absorbance of sample solution, Abs $_{blank}$ is the absorbance of blank, Slope is the "a" and "b" derived from the logarithmic equation (y = aLn (x) + b) of the BSA calibration curve plotted between concentrations and their corresponding absorbencies, and Amount $_{sample}$ is the amount of sample (mg).

2.5.6. Determination of starch (carbohydrates) content using iodine–starch test

Using a modified method of Chen et al. (2024), aqueous sample solutions were separately prepared and used to constitute the reaction mixture in a 96-well plate model, comprising of sample solution (or various concentrations of rice flour solutions) and 0.06 % I_2/KI reagent solution in a 1:1 *v*/v ratio. Absorbance was measured at 600 nm using a spectrophotometer. The starch content was calculated and presented as a percentage of starch in RTS. %Starch = [(Abs $_{sample}$ − Abs $_{blank}$) × 100] / (Slope × Amount $_{sample}$ (mg) x 1000), in which Abs $_{sample}$ is the absorbance of sample solution, Abs $_{blank}$ is the absorbance of blank, Slope is the "a" derived from the linear equation (y = ax) of the rice flour calibration curve plotted between concentrations and their corresponding absorbencies, and Amount $_{sample}$ is the amount of sample (mg).

2.5.7. Determination of fat content

The fat content of RTS was determined using a modified method from Tamprasit, Weerapreeyakul, Sutthanut, Thukhammee, and Wattanathorn (2019). Mixing exactly 1 g of RTS powder (Wsample) with 20 mL of n-hexane in a separatory funnel was shaken vigorously for 3 min, set until complete separation, and the extracted n-hexane layer was collected. Then, repeat the extraction of the RTS residue with another 20 mL of n-hexane. The collected n-hexane was pooled in a known-weight beaker (Wbeaker) and dried in a hot-air oven at 100 °C for 24 h until completely dried and got a constant weight (Wdried). The fat content was obtained following the equation %fat = [(Wdried (g) – Wbeaker (g)) × 100] / Wsample (g), then the result was expressed in an average of fat percentage.

2.6. Probiotic growth promoting

2.6.1. Culture medium preparation

A Bifidobacterium broth and agar plate were prepared following the manufacturer's direction. A 52-g bifidobacterium agar powder was dissolved in 1 L of distilled water, sterilized using an autoclave at 121 °C for 20 min, poured sterile bifidobacterium agar mixture into Petri dishes, dried in a hot-air oven at 70 °C, and stored in a refrigerator until used. An 82-g bifidobacterium broth powder was dissolved in 1 L of distilled water, sterilized using an autoclave at 121 °C for 20 min, and

stored in a refrigerator until used.

2.6.2. Microorganism culture and preparation

Bifidobacterium animalis colony in a bifidobacterium agar plate was prepared on a bifidobacterium agar after 24-h incubation under anaerobic conditions at 37 °C and used to prepare the culture stock probiotic for further experiments. The single colony of *B. animalis* was obtained from, inoculated into a 5-mL bifidobacterium broth, and incubated in an incubator shaker under anaerobic conditions at 37 °C for 8 h. Then, *B. animalis* inoculum suspension in bifidobacterium broth with a density of 10^6 CFU/mL was prepared as a stock culture for further experiments.

2.6.3. Probiotic enumeration by drop plate method

The prebiotic property of RTS was evaluated in an experiment of probiotic growth enhancement in response to RTS treatment at various concentrations compared to the controls—25 % *w/v* bifidobacterium broth and inulin, depicted by probiotic colony enumeration using a bacterial culture-based methodology followed by a plate count method (Hao, Esah, Tajarudin, Akter, & Mohd Salleh, 2021). Using a pre-optimized condition, the RTS sample (or 2.5 % inulin) solution prepared in 25 % *w/v* bifidobacterium broth at an optimal concentration range was mixed and co-cultured with 1-mL *B. animalis* stock culture in 25 % w/*v* bifidobacterium broth medium under anaerobic conditions at 37 °C of an incubator shaker for 8 h with a periodic sampling of 100 μL of the co-cultured mixture in every 3 h from 0 to 8 h period. Then, the sampling co-cultured mixture was enumerated for the probiotic population numbers by using the drop plate method; a 10-fold serial dilution in bifidobacterium broth 100 μL of each sampling mixture was prepared and dropped 10 μL onto the bifidobacterium agar plate in triplication. All dishes were incubated under anaerobic conditions at 37 °C for 48 h. Then, colony formation was observed and reported as colony-forming units per milliliter (CFU/mL).

2.7. Probiotic biofilm formation enhancement

2.7.1. Analysis of biofilm formation using crystal violet staining and spectroscopic method

Compared to the untreated control and inulin, the effect on biofilm formation of the RTS was determined using a modified method of Meza-Gutiérrez et al. (2022). The mixture of 200 μL of the inoculum, 1600 μL of 25 % *w/v* bifidobacterium broth medium, and 200 μL of the sample solution (RTS solution to make a desired concentration (1.25 %, 2.5 % or 5 % *w/v*) or 2.5 % inulin or 25 % w/v bifidobacterium broth for the control), was constituted in each well of a 24-well plate followed with 12-h incubation at 35–38 °C. After incubation, the supernatant of each well was removed and followed by normal saline solution rinsing before 20-min drying under hot airflow. Then, each was stained with a 2-mL 0.3 % crystal violet solution for 15 min, followed by distilled water rinsing and drying. Biofilm accumulations were observed and photographed under a light microscope. Subsequently, the stained biofilm in each well was dissolved with ethyl alcohol and measured the optical absorbance at 540 nm. As a result, the biofilm-forming index (BFI) was calculated following the equation: BFI = (As - Ab)/(Ac - Ab), in which As is the absorbance of the treatment group at 540 nm, Ac is the absorbance of the control group at 540 nm, and Ab is the absorbance of blank at 540 nm.

2.7.2. Identification of biofilm biomolecular composition using ATR-FTIR technique

Colonies from an 8-h co-culture of *B. animalis* probiotic bacteria with different concentrations of RTS powder and controls (bifidobacterium broth and inulin) in bifidobacterium broth were prepared in a bifidobacterium agar plate and used to characterize the biofilm formation. Then, biofilm biomolecular composition was identified using the ATR-FTIR technique (4500 Series, Agilent Technologies, CA, USA) to obtain the ATR-FTIR spectra of biofilm by placing a colony of *B. animalis* from each treatment (RTS or inulin or control) onto a crystal window and dried with a hot air dryer, then recorded the spectra in the wavenumber range of 650–4000 cm^{-1} with an average six scans. The MicroLab PC software was connected with Agilent 4500 Series FTIR spectrometers and was used for instrumental control. Spekwin 32 software was used for data acquisition and normalization. The FTIR spectra were analyzed to identify biofilm components by comparing them with the biofilm reference spectrum reported by Bosch et al. (2006) and Gieroba et al. (2020).

2.7.3. Classification of biofilm samples using principal component analysis

To indicate the significant variation of the biofilm's biological composition in response to the RTS treatment compared to the control, principal component analysis (PCA) (Unscrambler 9.7, CAMO Software AS, Oslo, Norway) was used to analyze the normalized FTIR spectral data from all samples in averaged six spectra over the wavenumber range of 650–4000 cm^{-1}. PCA scores from primary spectral RTS-treated, inulin-treated, and untreated (control) *B. animalis*' biofilm group were plotted to classify the sample groups based on their biofilm composition (supplementary Table S2). Loading plot analysis of principal component-1 (PC-1) and − 2 (PC-2) and correlation loadings were computed, and variables in the inner and outer ellipse indicated the 50 % and 100 % explained variance, respectively. Loading score and correlation loadings of PC-1 and PC-2 of each specific biological component were used to identify the variation of particular biological components between sample groups at specific assigned wavenumber ranges for protein (777–3283 cm^{-1}), fat (1398–2957 and 1072–1236 cm^{-1}), carbohydrate (1025–1114 cm^{-1}), and sugar (857–1078 cm^{-1}) (Bosch et al., 2006; Gieroba et al., 2020) (Table 5). Spectragryph software was employed in the peak area and average wavenumber analysis of each group spectra from 6 scans. The peak area was integrated from primary (raw data) spectral bands in the region of (i) amide A: 3250–3308 cm^{-1}, (ii) amide I: 1647–1653 cm^{-1}, (iii) amide II: 1480–1580 cm^{-1}, (iv) amide III: 1200–1350 cm^{-1}, (v) fats 1: 2800–3000 cm^{-1}, (vi) fats 2: 1350–1480 cm^{-1}, (vii) fats 3: 1200–1260 cm^{-1}, (viii) fats 4: 1060–1100 cm^{-1}, (ix) carbohydrates: 900–1200 cm^{-1}, (x) sugar: 850–1100 cm^{-1}, and secondary derivative spectral using the Savitzky-Golay algorithm in the region of (xi) carboxylic hydroxy (OH): 3040–3090 cm^{-1}, a chosen unoverlapping region to alcoholic OH (Kassem et al., 2023). For each sample group (RTS and inulin), the area under the curve (AUC) was determined by averaging the area of each absorption band, and these AUC values were then compared to those of the untreated control group.

2.8. Statistical analysis

All experiments were done at least in triplication, and the results were expressed as mean ± standard deviation (SD). The data were analyzed using SPSS version 19 statistical software program by Shapior-Wilk test of normality data distribution. Data sets with normal distribution with skewness within ±1 underwent a one-way analysis of variance (ANOVA) with Tukey Test multiple comparison tests. In contrast, non-normal distribution data sets were analyzed by using the Kruskal-Wallis test. Pearson's correlation coefficient was computed by the Bivariate Correlations from SPSS software. The significance was taken at a *p*-value less than 0.05 (p-value <0.05).

3. Results and discussion

3.1. Yields, nutrition composition, and physicochemical properties

Tamarind seed kernel powder (RTS) yielded 65.65 % (*w*/w), exhibiting water absorption ability (6.43 ± 0.54) and a swelling index of (0.56 ± 0.00). ATR-FTIR spectroscopy confirmed the presence of glucose, carbohydrates, fats, sugars, proteins, pectin, and xyloglucan (Glassford, Byrne, & Kazarian, 2013) (Fig. 1). Quantitative analysis revealed that fat (7.33 ± 0.03 %) and non-reducing sugars (3.57 ± 0.01

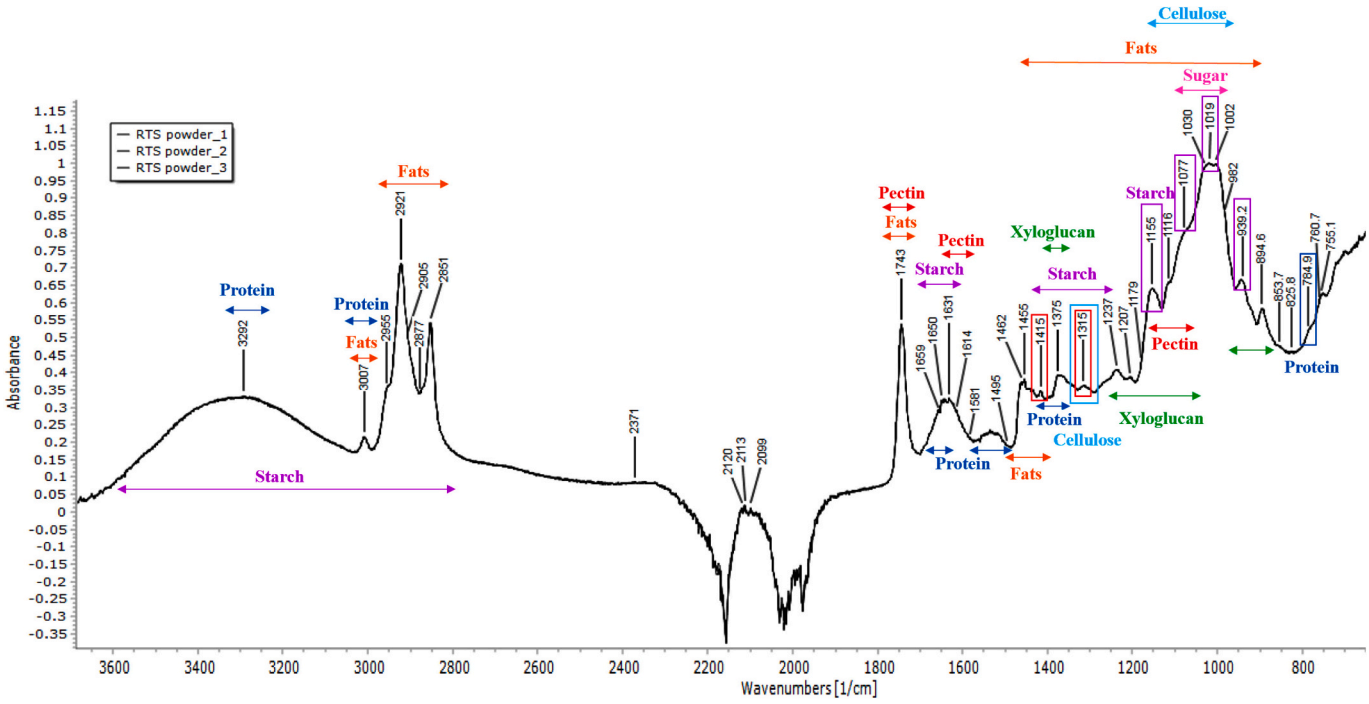

Fig. 1. The FTIR spectrum of RTS powder displays specific nutrition absorption bands, including starch (purple), protein (blue), fats (orange), pectin (red), xyloglucan (green), sugar (pink), and cellulose (light blue), identified according to the reference absorption bands designated for specific functional groups of nutrition components (Supplementary **Table S1**). (For interpretation of the references to colour in this figure legend, the reader is referred to the web version of this article.)

%) are the predominant components, followed by starch (0.76 %) and protein (0.25 %), with negligible reducing sugars. The RTS powder also contains phenolics (16.18 ± 0.54 mg catechin equivalents/g) and flavonoids (0.11 ± 0.02 mg quercetin equivalents/g). However, it shows negligible antioxidant activity (IC_{50} > 4000 μg/mL) compared to ascorbic acid (IC_{50} 11.89 ± 0.03 μg/mL; Table 1), and low reducing power in the DPPH assay indicated minimal antibacterial activity.

These findings align with previous reports describing tamarind seed kernel as a nutritionally rich source of carbohydrates, proteins, fats, and polysaccharide polymers (Kumar et al., 2008), although composition varies depending on origin, age, and processing. This contrasts with the tamarind seed coat, highly contained phenolics with the existence of heat-labile anti-nutritional phytic acid (Utami, Dewi, & Ningsih, 2022),

Table 1
Yield, physicochemical properties, phytochemical, and nutrition contents in the tamarind seed kernel (RTS) powder.

Yield (% *w/w* of tamarind seed)		65.65	
phytochemical properties*		nutrition composition*	
Water absorption index (WAI)	6.43 ± 0.54	Fat (%)	7.33 ± 0.03
Swelling index	0.56 ± 0.00	Non-reducing sugar (%)	3.57 ± 0.01
Total phenolic content (mg CE/g RTS powder) [a]	16.18 ± 0.54 (1.62 %)	Reducing sugar (%) [d]	Not detectable
Total flavonoid content (mg QE/g RTS powder) [b]	0.11 ± 0.02 (0.01 %)	Carbohydrate (starch) (%) [e]	0.76 ± 0.00
IC_{50} (μg/mL) [c]	> 4000	Protein (%) [f]	0.25 ± 0.00

* The average and standard deviation were calculated from values of independent testing triplication, which each value was extrapolated from a linear calibration curve of the corresponding reference standard compound: [a] catechin (y = 0.0157×, R^2 = 0.9990) and expressed as milligram catechin equivalence (CE); [b] quercetin (y = 0.0746×, R^2 = 0.9999) and expresses as milligram quercetin equivalence (QE); [c] Ascorbic acid (y = 4.2068, R^2 = 0.9992 with 50 % antioxidation inhibitory concentration (IC_{50}) = 11.89 ± 0.03 μg/mL; [d] D-glucose (y = 0.0259×, R^2 = 0.9997); [e] rice flour (y = 0.0015×, R^2 = 1); [f] bovine serum albumin (y = 0.0224ln(x) - 0.033, R^2 = 0.9913), respectively.

possesses bactericidal activity, and exhibits high reductive potential *via* its hydroxyl (OH) moieties, impacting Gram-positive bacterial cell membranes (Oulahal & Degraeve, 2022; Wandee et al., 2022).

The prebiotic potential of RTS is suggested by its nutritional composition. Carbohydrates, proteins, and fats contribute to prebiotic function in various foods (grains, vegetables, fruits). Fats support probiotic colonization and intestinal adhesion by increasing fatty acid production and lipid metabolism, leading to polyunsaturated fatty acid formation (*e.g.*, arachidonic and linolenic acid) (Kankaanpää, Salminen, Isolauri, & Lee, 2001). Furthermore, carbohydrates (including non-reducing sugars, mono- and oligosaccharides, FOS, XOS, GOS, and dietary fibers like inulin, hemicellulose, pectin, and xylans) are well-known for promoting probiotic growth and fermentation in the human gut (Hao et al., 2021; Hurtado-Romero et al., 2020). Proteins and amino acids generate beneficial short-chain fatty acids (SCFAs; butyrate, acetate, propionate) through fermentation (Hurtado-Romero et al., 2020).

The report of a high content of xyloglucan in tamarind seed kernel (65–72 %), a water-soluble fiber with prebiotic activity and intestinal mucous membrane barrier protective properties (Nguyen, Jittanit, & Srichamnong, 2019; Piqué, Gómez-Guillén, & Montero, 2018; Zhou et al., 2024), along with its water absorbability (WAI 6.43 ± 0.54) (Fig. 1 and Table 1), further supports its prebiotic potential.

Extract yield, water absorption, phytochemical components, and nutritional content are essential factors when assessing the potential of natural products, such as plant-derived functional foods in promoting the growth of probiotics and biofilm formation. Collectively, these factors play a synergistic role in enhancing the efficacy of functional foods or extracts in promoting probiotic growth and biofilm formation. Therefore, this information will be fundamental data for the further development of prebiotic standardization. In addition, understanding and optimizing these characteristics can improve the development of functional foods with enhanced probiotic benefits.

3.2. Growth-promoting activity

Table 2 shows that tamarind seed kernel powder (RTS) significantly

Table 2
The population numbers of *B. animalis* (A), their corresponding propagation rates (B) at various incubation periods following RTS treatment.

(A)

Sample	Numbers of *B. animalis* (CFU/ml) at each time point			
	0 h	3 h	6 h	8 h
RTS 5 %	3.50×10^4	9.02×10^5 †	2.50×10^8 *,†	4.00×10^{10} *,†
RTS 2.5 %	1.50×10^4	1.25×10^6 †	1.00×10^8 *,†	5.44×10^9 *,†
RTS 1.25 %	1.67×10^4	6.00×10^5 †	6.33×10^7 *,†	5.33×10^8 *,†
Control	1.00×10^4	8.33×10^5 †	2.06×10^7 †	2.00×10^8†
Inulin 2.5 %	9.67×10^4	5.67×10^6 †	1.00×10^{10} *,†	1.00×10^{12} *,†

(B)

Sample	Propagation or growth rate (%· h^{-1}) at each incubation period		
	0–3 h	3–6 h	6–8 h
RTS 5 %	11.26 ± 1.07 *	17.95 ± 1.26 *, †	22.54 ± 4.45 *, †
RTS 2.5 %	15.40 ± 1.11	15.39 ± 1.11 *	20.04 ± 3.47 *, †
RTS 1.25 %	12.84 ± 1.21 *	16.29 ± 0.45 *, †	11.08 ± 1.08 †
Control	16.67 ± 0.00	11.69 ± 0.76 †	12.49 ± 1.58 †
Inulin 2.5 %	11.83 ± 0.31 *	21.73 ± 0.31 *, †	20.07 ± 0.00 *, †

* indicates a significant difference ($p < 0.05$) compared to the control of each time point or period (within column comparison).
† indicates a significant difference ($p < 0.05$) compared to the origin (at 0 h time point or 0–3 h period) of each treatment (within row comparison).

stimulated *B. animalis* growth in a time- and concentration-dependent manner and comparable activity to the inulin (2.5 %) is found in the 2.5 and 5 % RTS treatment. After 6–8 h, substantial increases in *B. animalis* growth in response to the RTS treatment are demonstrated with significantly higher than the control (2.00×10^8 CFU/mL); with total population numbers of 5.33×10^8, 5.44×10^9, and 4.00×10^{10} CFU/mL for 1.25, 2.5, and 5 % RTS group, respectively (Table 2 **A** and supplementary Fig. S3). However, the unexpectedly lower growth rate in the treatment groups of 1.25 % and 5 % RTS and inulin during the initial (0−3 h) period is observed, and attribution of the increased viscosity and density of the culture medium is assumed to lead to interference in bacterial cells interaction and proliferating initiation (Sklodowska et al., 2018). However, this event recovers within 3 h of incubation, and then their growth-promoting activity can be exerted later. Compared to the control (without RTS, growth rate = 11.69 ± 0.76 %·h^{-1}), the RTS and inulin treatments significantly increase the growth rate during 3–8 h incubation. Meanwhile, 2.5 % RTS shows a high growth rate (15.40 ± 1.11 %·h^{-1}) during the early (0–3 h) incubation period. The observed effects are likely associated with complexity attributes, such as the nutritional and phytochemical composition and content, viscosity, and incubation duration.

Notably, in the 6–8 h incubation, the dose-dependent growth rate increase is manifested, with 5 % RTS showing the highest rate (22.54 ± 4.45 %·h^{-1}), followed by 2.5 % (20.04 ± 3.47 %·h^{-1}) and 1.25 % RTS (11.08 ± 1.08 %·h^{-1}). Among them, the 5 % and 2.5 % RTS groups show sustained growth rate increases, similar to inulin (a reference prebiotic) with *B. animalis* population numbers as high as 10^{10}–10^{12} CFU/mL. In contrast, the 1.25 % RTS and control groups show decreased growth rates after 6–8 h, similar to the control (*B. animalis* population numbers of 10^8 CFU/mL) (Table 2 **A and 2B**). The data presented in Fig. 2 clearly illustrates the notable increase in overall growth rates of 2.5 % and 5 % in the RTS- and inulin-treated groups compared to the control group. These findings suggest that RTS possesses prebiotic properties, stimulating *B. animalis* growth and accelerating its growth rate in a dose-dependent manner, similar to inulin. Additionally, the efficacy of prebiotic activity is determined by the presence of an adequate and optimal concentration of RTS.

3.3. Biofilm formation enhancement

The formation of *B. animalis* biofilm among the different treatments was demonstrated by colony characteristics and crystal violet staining intensity. This evidence indicates a greater capacity in enhancing biofilm formation in the *B. animalis* colonies in response to the tamarind seed kernel powder (RTS) treatment compared to the inulin-treated and control groups, leading to a significantly noticeable larger, brilliant, and expanding edge of the colonies (Fig. 3A). These results have been further confirmed using crystal violet staining to visualize and quantify the biofilm formation in expression by the biofilm formation index (BFI). The results demonstrate significantly enhanced *B. animalis* biofilm formation of the RTS in a dose-dependent manner, exceeding that of inulin

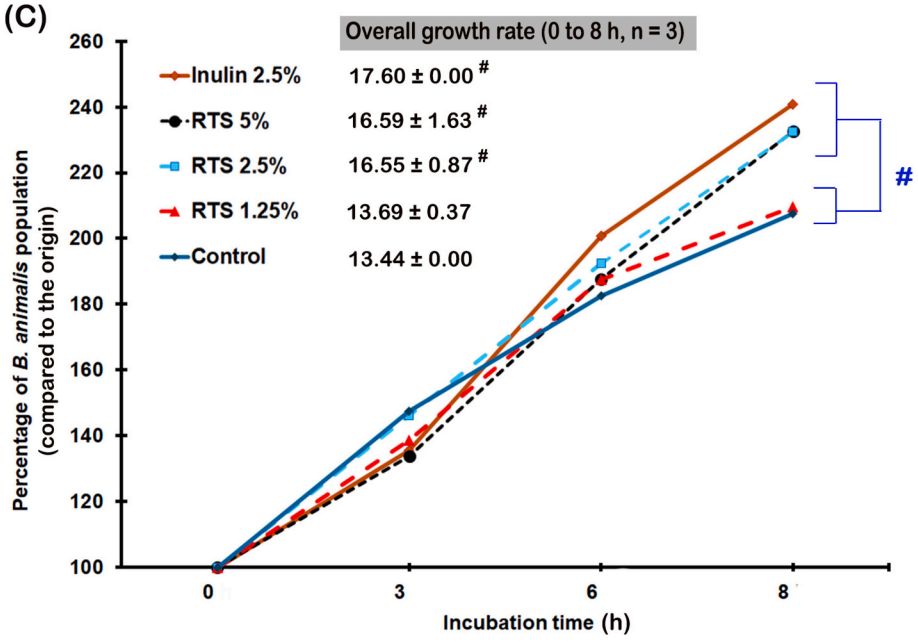

Fig. 2. The overall growth rates in the tamarind seed kernel powder (RTS), inulin, and control groups are presented, with the "#" symbol indicating a statistically significant difference ($p < 0.05$) compared to the control group.

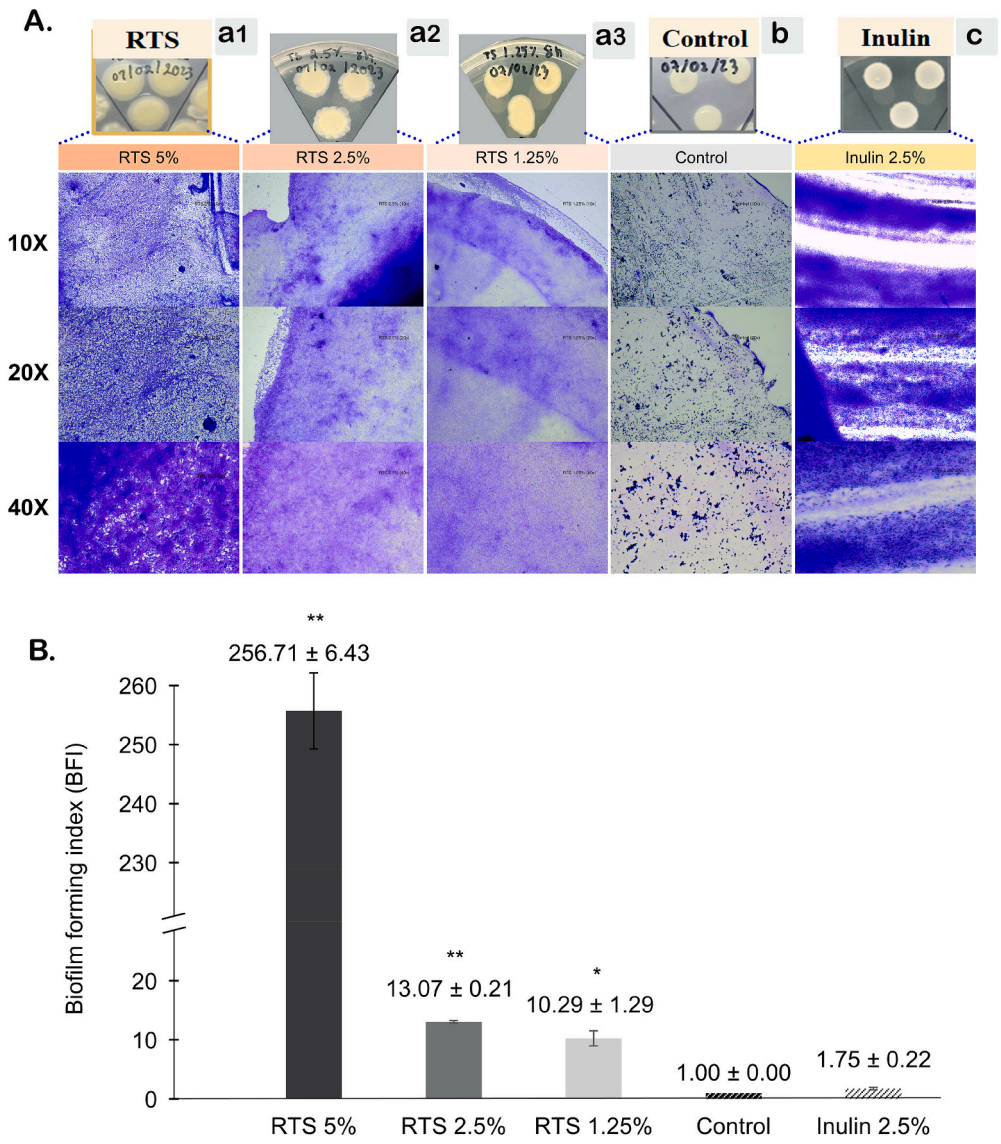

Fig. 3. The *B. animalis* colony characteristics (A) after treatment of tamarind seed kernel (RTS) (a1-a3), control (b), inulin (c), and their corresponding crystal violet stained biofilm under a light microscope at various magnifications (10×, 20×, and 40×) and biofilm-forming index (B) after RTS treatment at various concentrations were manifested in a dose-dependent manner with statistical significance when compared to the control and inulin 2.5 % (positive control) (* *p*-value <0.05, ** p-value <0.01). (For interpretation of the references to colour in this figure legend, the reader is referred to the web version of this article.)

and control groups; the 5 % RTS treatment is more effective than the 2.5 % and 1.25 % RTS, and inulin. This magnificent activity in the 5 % RTS group is depicted by the dense and fully occupied area of the crystal violet stained biofilm layer with the highest BFI (256.71) compared to the control (Fig. 3B).

RTS significantly enhances *B. animalis* biofilm formation in a dose-dependent manner (Fig. 3), exceeding the effect of 2.5 % inulin on an equivalent concentration basis. This highlights the importance of RTS's multi-nutritional composition and particular types of nutrition and ratios in promoting biofilm formation, which leads to a mechanism distinct from fructan-based inulin (Wan et al., 2020).

The prebiotic property of tamarind seed kernel powder, which encompasses a diverse array of nutrients including fat, non-reducing sugar, starch, protein, and dietary fibers, has been significantly demonstrated in its ability to promote the growth of *B. animalis* in a dose-dependent manner, along with a notable enhancement in biofilm formation observed within 6–8 h post-treatment. This implies the potential prebiotic activity of the tamarind seed kernel powder by promoting the proliferation of probiotics as the primary function and strengthening its efficacy by enhancing biofilm formation during the large intestinal transit time (Sensoy, 2021). The association is speculated to result from the diverse nutrient composition of tamarind seed kernel powder and their distinctive content ratios that collaboratively enhance prebiotic activity. This aligns with the report on the influence of nutrient type and quantity on biofilm formation: glucose and specific proteins like L-arginine and its metabolites are crucial for biofilm formation (Sauer et al., 2004; Scribani Rossi et al., 2022), carbohydrate effects on biofilm formation are complex, including pH reduction and the crucial role of non-reducing sugars like sucrose (Khangholi & Jamalli, 2016). In addition, fat can facilitate probiotic colonization and intestinal adhesion. This evidence has highlighted the potential benefits of the substantial fat levels observed in the tamarind seed kernel powder on its prebiotic activity (Kankaanpää et al., 2001). Nonetheless, the specific roles of various nutrients (carbohydrates, non-reducing sugars, proteins, polyunsaturated fatty acids) and their synergistic potential in probiotic biofilm formation and adhesion are still not fully understood. Consequently, further in-depth investigation is advisable to enhance the development of precise nutrition for targeted health benefits. In

addition, to elucidate the tamarind seed kernel powder impact on the biofilm biomolecular composition, characterization and differentiation among the resultant biofilm in response to various treatments based on their biomolecular composition and alterations is conducted using ATR-FTIR spectroscopy and PCA analysis.

3.4. Biofilm biomolecular composition characterization and differentiation

The employment of ATR-FTIR spectroscopy results in the distinctive FTIR spectra demonstrated their biomolecular composition variation of

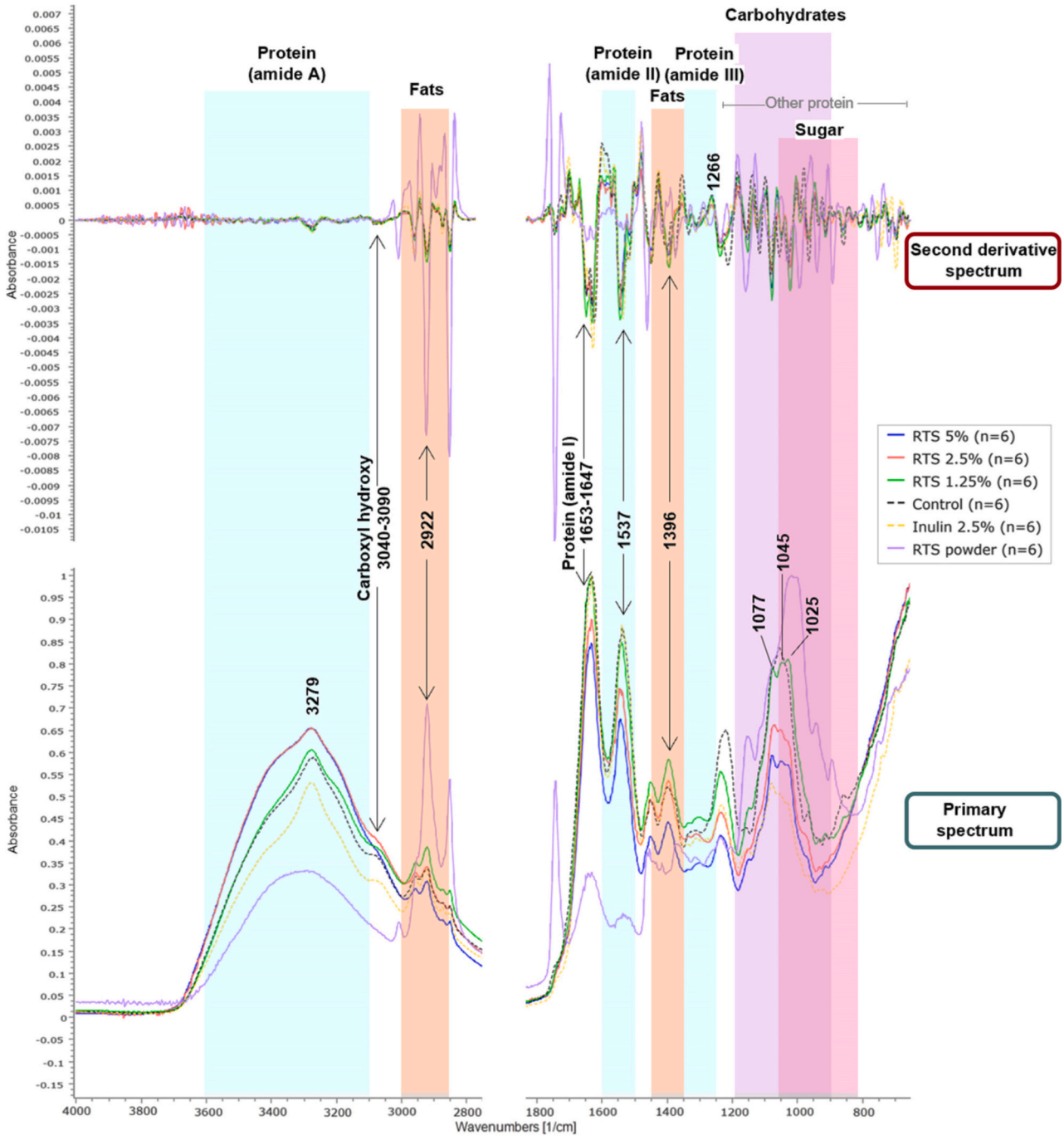

Fig. 4. The primary and the secondary derivative FTIR spectra of biofilm derived from a *B. animalis* single colony after tamarind seed kernel powder (RTS) treatment at concentrations of 1.25 % (Green), 2.5 % (Red), and 5 % (Blue) compared to the control group (Black) and inulin 2.5 % (Yellow) are illustrated, which remarkable distinct from the RTS FTIR spectrum (Pink) indicating the biomolecular compositions variation between the biofilm biological components of the biofilm and RTS powder. These are precisely investigated according to regions, including protein (Blue), fats (Orange), carbohydrates (Purple), and sugar (Pink). Protein regions (777–3283 cm^{-1}) were majorly presented at assigned wavenumber range as amide A (3261–3283 cm^{-1}), amide I (1647–1653 cm^{-1}), amide II (1537–1546 cm^{-1}), amide III (1301–1314 cm^{-1}), and other proteins include such DNA/RNA/phosphorylated protein (1236–967 cm^{-1}) and the vibration of tryptophan, tyrosine, and phenylamine ring (777–869 cm^{-1}). Fats regions were found in the vibration of the wavenumber range 1220–2957 cm^{-1} and 967–1236 cm^{-1} (phospholipids). Sugar regions (857–1079 cm^{-1}) are defined as the β-glucan bonds, D-glucose, D-glucan, and the glycosidic linkage type of anomeric region. In addition, the carboxylic hydroxy moiety (OH band) is depicted at 3040–3090 cm^{-1}. (For interpretation of the references to colour in this figure legend, the reader is referred to the web version of this article.)

the biofilm samples of the post-treatment of 2.5 % inulin, and various tamarind seed kernel powder (RTS) concentrations (1.25 %, 2.5 %, and 5 %) and the control (Fig. 4). Compared to the reference FTIR spectroscopic data of biofilm (Bosch et al., 2006; Gieroba et al., 2020), the composition of biological components in each biofilm sample was characterized according to the responsible functional group absorption bands in the assigned specific regions of protein (amide A, I, II, III; 777–3283 cm^{-1}), lipid (1220–2957 cm^{-1}, 967–1236 cm^{-1}), and carbohydrate regions (857–1079 cm^{-1}), differences are observed among treatments. RTS-treated groups show distinct peaks in the carbohydrate region (1073–1079 cm^{-1}, 1049–1051 cm^{-1}, 1025–1028 cm^{-1}) compared to the control (1081, 1055, and 1030 cm^{-1}), indicating alterations in sugar composition (β-glucan bonds, D-glucose, D-glucan, and anomeric regions) (Table 3). Notably, a carboxyl hydroxyl (OH) group is consistently detected at 3040–3090 cm^{-1} in the RTS-treated groups.

Principal component analysis (PCA) of the FTIR data (Unscrambler 9.7; CAMO Software AS, Oslo, Norway) clearly distinguishes the biofilm from control, inulin (2.5 %), and RTS-treated groups (Fig. 5A), PCA score plot with the principal component (PC)-1 (65 %, x-axis) and PC-2 (28 %, y-axis) accounting for 93 % of the data variability (Truong, Chapman, & Cozzolino, 2021). The PCA score plot (Fig. 5A) and correlation loading plot (Fig. 5B) illustrate the significant effect of RTS on biofilm composition, particularly highlighting differences in protein (amide A, I, II) and carbohydrate regions (Fig. 4 and Fig. 5B) compared to control and inulin (Fig. 5A). Specifically, higher RTS concentrations (2.5 % and 5 %) correlate with increased amide A (3200–3300 cm^{-1}) and decreased carboxylic hydroxyl (OH) (3040–3090 cm^{-1}) signals, differ from the control and 1.25 % RTS (Fig. 5B). This is further supported by Pearson's correlation analysis (Fig. 6B), showing strong positive correlations between RTS concentration, biofilm formation index (BFI), and amide A area under the curve (AUC) ($p < 0.001$), yet negative correlations with amide I, II, III, fats, and OH ($p < 0.05$). Unlike inulin, the distinct impact of RTS on the amide A functional group provides early evidence of prebiotic agent impact in *B. animalis* biofilm formation (Fig. 6A).

Biofilm represents a sophisticated extracellular matrix structure, intricately composed of extracellular DNA, proteins, and polysaccharides generated by microorganisms to facilitate surface attachment and self-envelopment. This structural composition enables microorganisms to withstand adverse environmental conditions and maintain a sessile metabolic state. Additionally, the biofilm's properties—such as mechanical strength, adhesion, and resistance to antimicrobial agents—are significantly influenced by hydrogen bonding interactions within the protein components of the extracellular matrix,

Table 3
FTIR absorption bands assigned the biological components in *B. animalis* formed-biofilm in the control and treatment of inulin or tamarind seed kernel (RTS) compared to the reference absorption bands.

Component	Wavenumber (cm^{-1})				Functional groups	Reference
	Assigned	Control	Treatment			
			Inulin	RTS		
Protein	3100–3600	3272	3275	3277–3280	ν (N—H) of Amide A	(Bosch et al., 2006; Gieroba et al., 2020)
	1650	1650	1652	1650	ν (C=O) and δ (C—N) of Amide *I*	(Bosch et al., 2006)
	1615–1627	1624	1627	1629	ν_{as} (C=O)	
	1500–1600	1536	1537	1536–1544	δ (N—H), ν (C—N), and ν (C—C) of Amide II	
	1441–1462	1454	1454	1451–1454	Pyrrolidine ring of proline and hydroxyproline	
	1400–1450	1428	1427	1428	as (CH_3) def, as (CH_2) def	(Gieroba et al., 2020)
	1350–1400	1398	1396	1396–1397	as (CH_3) def, as (CH_2) def, νs (C=O)	
	1200–1350	1263	1266	1265	δ (N—H), ν (C—N), δ (C=O), ν (C—C), ν (CH_3) of amide III	
	1220–1250	1220	1234	1235–1236	ν_{as} (PO^{2-}) of DNA, RNA, and phosphorylated proteins	(Bosch et al., 2006; Gieroba et al., 2020)
	1086	1081	1079	1072–1078		
	1009–1016	1002	1002	1003–1005	ν (C—C) of RNA	
	972	967	967	969–972	ν (C—C), ν (C—C) deoxyribose of DNA	(Gieroba et al., 2020)
	700–900	859, 809, 779	859, 831, 779	857–863, 809–810, 777	Anomeric ring vibrations of Trp, Tyr, and Phe	
Fats	2950–2960	2957	2959	2957	ν_{as} (CH_3)	(Gieroba et al., 2020)
	2920–2940	2922	2925	2922	ν_{as} (CH_2)	
	2875	2872	2873	2872–2873	ν_s (CH_3)	(Bosch et al., 2006)
	2850–2860	2849	2853	2851	ν_s (CH_2)	(Gieroba et al., 2020)
	1730–1745	1746	1741	1739–1741	ν (C=O)	(Bosch et al., 2006)
	1615–1627	1624	1627	1629	ν_{as} (C=O) of COO–	
	1400–1450	1454	1454	1451–1454	as (CH_3) def, as (CH_2) def	(Gieroba et al., 2020)
	1350–1400	1398	1396	1396–1397	as (CH_3) def, as (CH_2) def, νs (C=O)	
	1260	1263	1266	1265	ν (C-O-C) of ester	(Bosch et al., 2006)
	1220–1250	1220	1234	1235–1236	ν_{as} (PO^{2-}) of phospholipids	(Bosch et al., 2006; Gieroba et al., 2020)
	1086	1081	1079	1073–1079	ν_{as} (PO^{2-}) phospholipids	(Gieroba et al., 2020)
Carbohydrates	900–1200	1081, 1055, 1030	1079, 1053, 1030	1073–1079, 1049–1051, 1025–1028	(C-O-C), (C—O) of oligo, polysaccharide, and alginate)	(Bosch et al., 2006)
	1137–1144	1140	1138	1136–1140	Oligosaccharides	(Gieroba et al., 2020)
	1070–1080	1081	1079	1073–1079	ν (C—C) of β-glucan bonds	
Sugar	1046–999	1030	1030	1025–1028	Skeletal vibration connected to the anomeric structure of D-glucose	(Gieroba et al., 2020)
	1009–1016	1002	1002	1003–1005	ν (C—C) of ribose	
	929	933	933	931–933	(1 → 3)-a-D-glucan	
	800–900	859	859	857–863	Glycosidic linkage type of anomeric region	(Bosch et al., 2006)
	852–860	859	859	857–863	(1 → 3),(1 → 6)-a-D-glucan	(Gieroba et al., 2020)

Type of vibrations: stretching (ν), bending (δ), twisting (τ), wagging (w), scissoring (σ), deformation (def), symmetrical (s), and asymmetrical (as) mode. Control: the wavenumber ranges from *B. animalis* biofilm without any additional treatment. RTS-treated: the wavenumber ranges from *B. animalis* biofilm with RTS powder (1.25, 2.5, and 5 %) treatment.

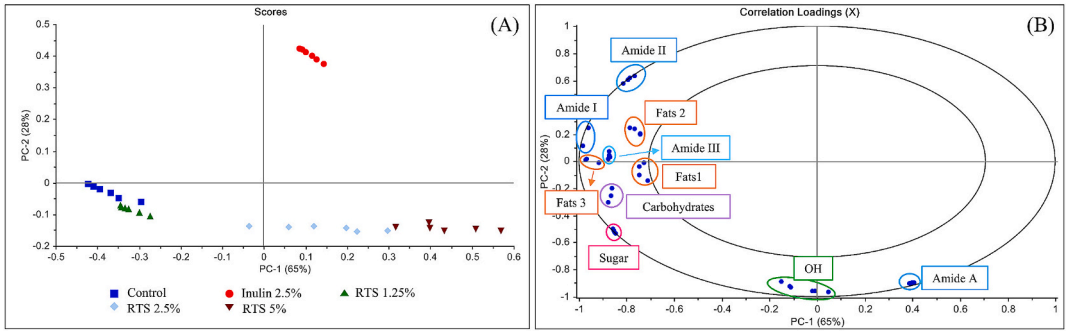

Fig. 5. Principal component analysis (PCA) score plot (A) of primary FTIR spectra of *B. animalis*' biofilm resulted after treatment of tamarind seed kernel (RTS) at 1.25, 2.5, and 5 %, inulin 2.5 %, and untreated (control) group and correlation loading plots (B) of specific nutrition component wavenumbers of protein: amide A, amide I, amide II, and amide III (Blue), fats (Orange), carbohydrates (Purple), sugar (Pink), and carboxylic hydroxy (OH) (Green) bands that contribute to discrimination among the biofilm sample groups. (For interpretation of the references to colour in this figure legend, the reader is referred to the web version of this article.)

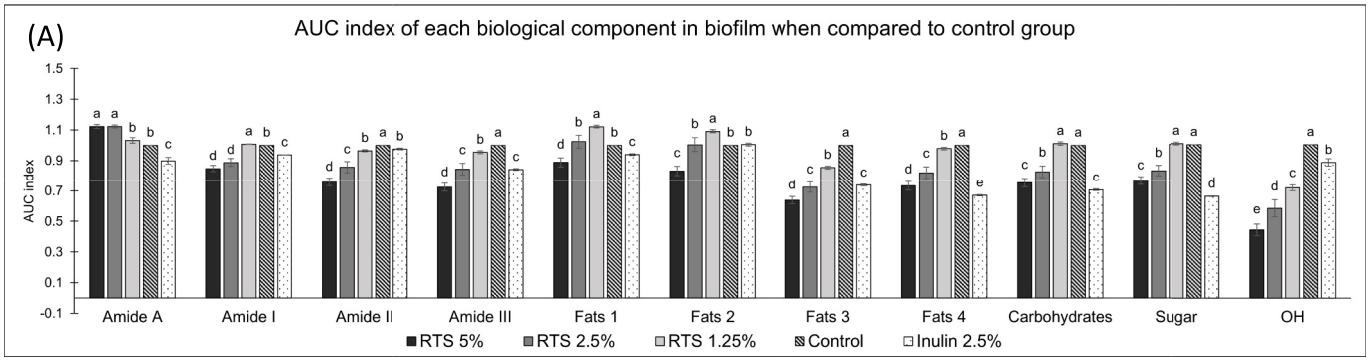

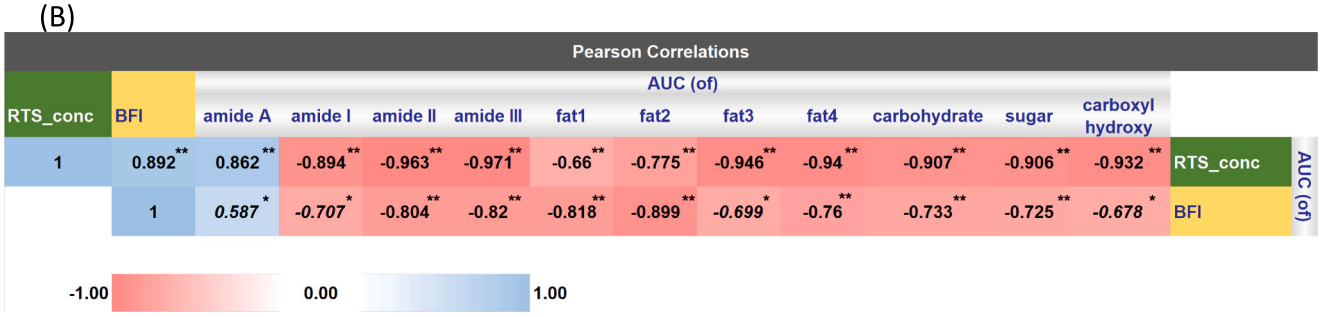

Fig. 6. The clustered bar graph illustrates the average area under the curve (AUC) index ($n = 6$) (A) of FTIR absorption bands at specific wavelength numbers for each biological component functional group. This representation highlights the variation in biomolecular composition among the resultant biofilm in response to the RTS and inulin treatment compared to the control (untreated) group. The findings demonstrate statistical significance, indicated by p-values <0.05 for factors a, b, c, d, and e. In addition, Pearson's correlations (B) show the significant influence of RTS concentration on the biofilm biomolecular characteristics. The positive correlations were observed with the biofilm-forming index (BFI) and the area under the curve (AUC) of the amide A functional group of the protein is evidenced, while negative correlations with others are illustrated (AUC of amide I, amide II, amide III, fat1, fat2, fat3, and carboxylic hydroxy functional group of the biofilm FTIR absorption region) (* p-value <0.05, ** p-value <0.01).

which are critical for maintaining structural integrity. Notably, the amide A functional group plays a pivotal role in forming hydrogen bonds with neighboring biomolecules, essential for biofilm formation and adherence. Specifically, the carbonyl oxygen (C═O, at 1300–1400 cm^{-1}) acts as a hydrogen bond acceptor, while the amine hydrogen (N—H, at 3300–3500 cm^{-1}) serves as a hydrogen bond donor. Consequently, this bonding contributes to the stability and cohesive structure of the biofilm, enhancing probiotic stability and functionality while reducing susceptibility to antimicrobial agents (Blackman, Qu, Cass, & Locock, 2021).

The data compellingly demonstrate that tamarind seed kernel powder exerts a multifaceted influence on *B. animalis* propagation and biofilm formation, impacting not only the quantity (overall population and biofilm biomass) but also the quality of the biofilm matrix. This is evidenced by significant alterations in the biomolecular composition, and implied structural organization of the biofilm, as revealed by the combined ATR-FTIR and PCA analyses that offer a potential method for rapid, non-destructive assessment of tamarind seed kernel powder efficacy in future studies. This analytical approach proves highly valuable for characterizing prebiotic-induced biofilm modifications, offering a detailed understanding of how prebiotics interact with bacterial communities. Notably, the identification of specific wavenumbers associated with amide A N—H bending as a potential hallmark of tamarind seed kernel powder-induced biofilm formation in *B. animalis* warrants further

investigation. This finding presents an opportunity to deepen our understanding of the underlying impacts and mechanisms involved in biofilm development.

In addition to its evident prebiotic property, the distinctive traits of tamarind seed kernel greatly improve the prospects for tamarind seed kernel powder applications. The impressive safety profile, along with its pleasant taste, cost-effectiveness, broad availability, and stability, make tamarind seed kernel powder a compelling option for consideration in the development of functional food ingredients or dietary supplements. The noted increase in beneficial bacterial growth and biofilm formation indicates that tamarind seed kernel powder may play a role in improving gut health. The result of this study is an important step forward in advancing the understanding of prebiotic mechanisms and identifying new, sustainable, and cost-effective potential of local ingredients to enhance gut health through dietary interventions. Moreover, this evidence is paving the way for the development of tamarind seed kernel powder-based probiotic products in various forms and functional food ingredients with a feature of prebiotics to enrich specific bacterial groups in the gut. However, it is crucial to acknowledge that these encouraging *in vitro* results require additional confirmation through *in vivo* studies to completely validate the positive impacts of tamarind seed kernel powder on gut health and to apply these findings effectively in food and health products.

4. Conclusion

Tamarind seed kernel powder has been discovered as a potential prebiotic agent, significantly promoting the growth and biofilm formation of *Bifidobacterium animalis* in a dose-dependent manner, especially at concentrations of 2.5 % and 5 %. This effect is comparable to that of inulin, but it uniquely surpasses inulin in enhancing biofilm formation, which is crucial for the successful colonization of probiotics in the gut. Moreover, the powder induces specific changes in the biomolecular composition of *B. animalis* biofilms, as validated by ATR-FTIR and PCA analyses. Notably, there is an increase in amide A and a decrease in hydroxyl groups. Its prebiotic capacity is further supported by a diverse nutritional profile that includes carbohydrates, proteins, and fats, which differs from the fructan-based inulin. This highlights the importance of its unique composition and ratios for the prebiotic activity. These findings open promising avenues for further research into the underlying mechanisms of Tamarind seed kernel powder and emphasize its potential applications in developing novel and effective dietary supplements to improve gut health and overall wellness.

CRediT authorship contribution statement

Roongrawee Wandee: Writing – original draft, Visualization, Software, Methodology, Investigation. **Khaetthareeya Sutthanut:** Writing – review & editing, Writing – original draft, Validation, Supervision, Software, Methodology, Investigation, Formal analysis, Data curation, Conceptualization. **Jenjira Songsri:** Software, Methodology, Investigation. **Natthida Weerapreeyakul:** Writing – review & editing, Validation. **Theera Rittirod:** Resources. **Patcharaporn Tippayawat:** Validation, Methodology. **Orawan Yangkruea:** Investigation. **Sirapop Jakcharoenpornchai:** Investigation.

Declaration of competing interest

The authors declare that they have no known competing financial interests or personal relationships that could have appeared to influence the work reported in this paper.

Acknowledgments

This research was supported by the Research Administration Division (Research and Graduate Studies) through the Research Program and the Fundamental Fund of Khon Kaen University and the National Science, Research and Innovation Fund (NSRF).

Appendix A. Supplementary data

Supplementary data to this article can be found online at https://doi.org/10.1016/j.fochx.2025.102180.

Data availability

All relevant data are within the paper and its supporting file. Any further datasets are available from the corresponding author.

References

Anderson, R. A., Conway, H. F., & Peplinski, A. J. (1970). Gelatinization of corn grits by roll cooking, extrusion cooking and steaming. *Starch - Stärke, 22*(4), 130–135. https://doi.org/10.1002/star.19700220408

Arboleya, S., Watkins, C., Stanton, C., & Ross, R. P. (2016). Gut bifidobacteria populations in human health and aging. *Frontiers in Microbiology, 7*, 1204.

Blackman, L. D., Qu, Y., Cass, P., & Locock, K. E. S. (2021). Approaches for the inhibition and elimination of microbial biofilms using macromolecular agents. *Chemical Society Reviews, 50*(3), 1587–1616. https://doi.org/10.1039/D0CS00986E

Bosch, A., Serra, D., Prieto, C., Schmitt, J., Naumann, D., & Yantorno, O. (2006). Characterization of Bordetella pertussis growing as biofilm by chemical analysis and FT-IR spectroscopy. *Applied Microbiology and Biotechnology, 71*(5), 736–747. https://doi.org/10.1007/s00253-005-0202-8

Chen, L., Li, X., Li, W., Hao, X., Wu, S., Zhang, M., & Zhang, N. (2024). Structural, physicochemical, and digestive properties of enzymatic debranched rice starch modified by phenolic compounds with varying structures. *International Journal of Biological Macromolecules, 274*, Article 133262. https://doi.org/10.1016/j.ijbiomac.2024.133262

Davey Mary, E., & O'Toole George, A. (2000). Microbial biofilms: From ecology to molecular genetics. *Microbiology and Molecular Biology Reviews, 64*(4), 847–867. https://doi.org/10.1128/mmbr.64.4.847-867.2000

Day, R. L., Harper, A. J., Woods, R. M., Davies, O. G., & Heaney, L. M. (2019). Probiotics: Current landscape and future horizons. *Future Science OA, 5*(4), FSO391. https://doi.org/10.4155/fsoa-2019-0004

Deeyai, P., Suphantharika, M., Wongsagonsup, R., & Dangtip, S. (2013). Characterization of modified tapioca starch in atmospheric argon plasma under diverse humidity by FTIR spectroscopy. *Chinese Physics Letters, 30*, Article 018103. https://doi.org/10.1088/0256-307X/30/1/018103

Gieroba, B., Krysa, M., Wojtowicz, K., Wiater, A., Pleszczyńska, M., Tomczyk, M., & Sroka-Bartnicka, A. (2020). The FT-IR and Raman spectroscopies as tools for biofilm characterization created by cariogenic streptococci. *International Journal of Molecular Sciences, 21*(11). https://doi.org/10.3390/ijms21113811

Glassford, S. E., Byrne, B., & Kazarian, S. G. (2013). Recent applications of ATR FTIR spectroscopy and imaging to proteins. *Biochimica et Biophysica Acta, 1834*(12), 2849–2858. https://doi.org/10.1016/j.bbapap.2013.07.015

Hamuel, J. D. (2007). Antimicrobial activity of Tamarindus indica Linn. *Tropical Journal of Pharmaceutical Research, 5 Num 2*, 5. https://doi.org/10.4314/tjpr.v5i2.14637 (ISSN: 1596-5996).

Hao, C., Esah, E., Tajarudin, H., Akter, B., & Mohd Salleh, R. (2021). Effect of potential prebiotics from selected fruits Peel on the growth of probiotics. *Journal of Food Processing and Preservation, 45*. https://doi.org/10.1111/jfpp.15581

Hurtado-Romero, A., Del Toro-Barbosa, M., Garcia-Amezquita, L. E., & García-Cayuela, T. (2020). Innovative technologies for the production of food ingredients with prebiotic potential: Modifications, applications, and validation methods. *Trends in Food Science & Technology, 104*, 117–131. https://doi.org/10.1016/j.tifs.2020.08.007

Kaewkumsan, P., & Hongsawadee, B. (2014). The use of tamarind kernel powder substitute commercial pectin. *Khon Kaen Agric. J., 42*, 641–645.

Kankaanpää, P. E., Salminen, S. J., Isolauri, E., & Lee, Y. K. (2001). The influence of polyunsaturated fatty acids on probiotic growth and adhesion. *FEMS Microbiology Letters, 194*(2), 149–153. https://doi.org/10.1111/j.1574-6968.2001.tb09460.x

Kassem, A., Abbas, L., Coutinho, O., Opara, S., Najaf, H., Kasperek, D., & Tiquia-Arashiro, S. (2023). Applications of Fourier transform-infrared spectroscopy in microbial cell biology and environmental microbiology: Advances, challenges, and future perspectives. *Frontiers in Microbiology, 14*, 1304081. https://doi.org/10.3389/fmicb.2023.1304081

Khangholi, M., & Jamalli, A. (2016). The effects of sugars on the biofilm formation of Escherichia coli 185p on stainless steel and polyethylene terephthalate surfaces in a laboratory model. *Jundishapur Journal of Microbiology, 9*(9), Article e40137. https://doi.org/10.5812/jjm.40137

Kizil, R., Irudayaraj, J., & Seetharaman, K. (2002). Characterization of irradiated starches by using FT-Raman and FTIR spectroscopy. *Journal of Agricultural and Food Chemistry, 50*(14), 3912–3918. https://doi.org/10.1021/jf011652p

Kong, J., & Yu, S. (2007). Fourier transform infrared spectroscopic analysis of protein secondary structures. *Acta Biochimica et Biophysica Sinica, 39*(8), 549–559.

Koruri, S. S., Banerjee, D., Chowdhury, R., & Bhattacharya, P. (2014). Studies on prebiotic food additive (inulin) in Indian dietary fibre sources - garlic (Allium

sativum), wheat (Triticum spp.), oat (Avena sativa) and dalia (bulgur). *International Journal of Pharmacy and Pharmaceutical Sciences, 6*, 278–282.

Kumar, C. S., & Bhattacharya, S. (2008). Tamarind seed: Properties, processing and utilization. *Critical Reviews in Food Science and Nutrition, 48*(1), 1–20. https://doi.org/10.1080/10408390600948600

Liu, Z., Li, L., Fang, Z., Lee, Y., Zhao, J., Zhang, H., & Lu, W. (2021). The biofilm-forming ability of six Bifidobacterium strains on grape seed flour. *LWT, 144*, Article 111205. https://doi.org/10.1016/j.lwt.2021.111205

Lugli, G. A., Mancino, W., Milani, C., Duranti, S., Mancabelli, L., Napoli, S., & Turroni, F. (2019). Dissecting the evolutionary development of the species Bifidobacterium animalis through comparative genomics analyses. *Applied and Environmental Microbiology, 85*(7). https://doi.org/10.1128/aem.02806-18

Martens, K., Pugin, B., De Boeck, I., Spacova, I., Steelant, B., Seys, S. F., & Hellings, P. W. (2018). Probiotics for the airways: Potential to improve epithelial and immune homeostasis. *Allergy, 73*(10), 1954–1963. https://doi.org/10.1111/all.13495

Mehrotra, R. (2006). *Infrared spectroscopy*. In *Encyclopedia of Analytical Chemistry*: Gas Chromatography/Infrared in Food Analysis.

Meza-Gutiérrez, N. N., Magallón-Servín, P., Balois-Morales, R., Pérez-Ramírez, I. F., López-Guzmán, G. G., Berumen-Varela, G., & Bautista-Rosales, P. U. (2022). Growth promoting activity of Annona muricata L. *Leaf Extracts on Lactobacillus casei. Plants (Basel), 11*(5). https://doi.org/10.3390/plants11050581

Nguyen, T. T., Jittanit, W., & Srichamnong, W. (2019). Production of xyloglucan component extracted from tamarind (Tamarindus indica) seeds using microwave treatment for seed decortication. *Journal of Food Processing and Preservation, 43*(8), Article e14055. https://doi.org/10.1111/jfpp.14055

Nouvenne, A., Ticinesi, A., Tana, C., Prati, B., Catania, P., Miraglia, C., & Meschi, T. (2018). Digestive disorders and intestinal microbiota. *Acta Biomedica Atenei Parmensis, 89*(9-S), 47–51. https://doi.org/10.23750/abm.v89i9-S.7912

Ogura, I., Sugiyama, M., Tai, R., Mano, H., & Matsuzawa, T. (2023). Optimization of microplate-based phenol-sulfuric acid method and application to the multi-sample measurements of cellulose nanofibers. *Analytical Biochemistry, 681*, Article 115329. https://doi.org/10.1016/j.ab.2023.115329

Oulahal, N., & Degraeve, P. (2022). Phenolic-Rich Plant extracts with antimicrobial activity: An alternative to food preservatives and biocides? *Frontiers in Microbiology, 12*. https://doi.org/10.3389/fmicb.2021.753518

Piqué, N., Gómez-Guillén, M. D. C., & Montero, M. P. (2018). Xyloglucan, a plant polymer with barrier protective properties over the mucous membranes: An overview. *International Journal of Molecular Sciences, 19*(3), 673. https://www.mdpi.com/1422-0067/19/3/673.

Sauer, K., Cullen, M. C., Rickard, A. H., Zeef, L. A., Davies, D. G., & Gilbert, P. (2004). Characterization of nutrient-induced dispersion in Pseudomonas aeruginosa PAO1 biofilm. *Journal of Bacteriology, 186*(21), 7312–7326. https://doi.org/10.1128/jb.186.21.7312-7326.2004

Scribani Rossi, C., Barrientos-Moreno, L., Paone, A., Cutruzzolà, F., Paiardini, A., Espinosa-Urgel, M., & Rinaldo, S. (2022). Nutrient sensing and biofilm modulation: The example of L-arginine in Pseudomonas. *International Journal of Molecular Sciences, 23*(8), 4386. https://www.mdpi.com/1422-0067/23/8/4386.

Sensoy, I. (2021). A review on the food digestion in the digestive tract and the used in vitro models. *Current Research in Food Science, 4*, 308–319. https://doi.org/10.1016/j.crfs.2021.04.004

Sharma, L., & Riva, A. (2020). Intestinal barrier function in health and disease—Any role of SARS-CoV-2? *Microorganisms, 8*(11), 1744. https://www.mdpi.com/2076-2607/8/11/1744.

Sherovski, P., Stojković, G., & Ristovska, N. (2018). Development, validation and application of first derivative spectroscopy ratio method for estimation of Bradford assay. *Analytical Biochemistry, 558*, 35–40. https://doi.org/10.1016/j.ab.2018.07.027

Sklodowska, K., Debski, P. R., Michalski, J. A., Korczyk, P. M., Dolata, M., Zajac, M., & Jakiela, S. (2018). Simultaneous measurement of viscosity and optical density of bacterial growth and death in a microdroplet. *Micromachines, 9*(5), 251. https://www.mdpi.com/2072-666X/9/5/251.

Szymanska-Chargot, M., & Zdunek, A. (2013). Use of FT-IR spectra and PCA to the bulk characterization of Cell Wall residues of fruits and vegetables along a fraction process. *Food Biophysics, 8*(1), 29–42. https://doi.org/10.1007/s11483-012-9279-7

Tamprasit, K., Weerapreeyakul, N., Sutthanut, K., Thukhammee, W., & Wattanathorn, J. (2019). Harvest age effect on phytochemical content of white and black glutinous Rice cultivars. *Molecules, 24*(24), 4432. https://www.mdpi.com/1420-3049/24/24/4432.

Truong, V. K., Chapman, J., & Cozzolino, D. (2021). Monitoring the bacterial response to antibiotic and time growth using near-infrared spectroscopy combined with machine learning. *Food Analytical Methods, 14*(7), 1394–1401. https://doi.org/10.1007/s12161-021-01994-6

Utami, M., Dewi, A., & Ningsih, N. (2022). Potential of tamarind seeds (Tamarindus indica L.) as prebiotics on the growth of lactic acid bacteria. *IOP Conference Series: Earth and Environmental Science, 980*, Article 012017. https://doi.org/10.1088/1755-1315/980/1/012017

Wan, X., Guo, H., Liang, Y., Zhou, C., Liu, Z., Li, K., & Wang, L. (2020). The physiological functions and pharmaceutical applications of inulin: A review. *Carbohydrate Polymers, 246*, Article 116589. https://doi.org/10.1016/j.carbpol.2020.116589

Wandee, R., Sutthanut, K., Songsri, J., Sonsena, S., Krongyut, O., Tippayawat, P., & Rittirod, T. (2022). Tamarind seed coat: A Catechin-rich source with anti-oxidation, anti-Melanogenesis, anti-Adipogenesis and anti-microbial activities. *Molecules, 27*(16). https://doi.org/10.3390/molecules27165319

Wood, I. P., Elliston, A., Ryden, P., Bancroft, I., Roberts, I. N., & Waldron, K. W. (2012). Rapid quantification of reducing sugars in biomass hydrolysates: Improving the speed and precision of the dinitrosalicylic acid assay. *Biomass and Bioenergy, 44*, 117–121. https://doi.org/10.1016/j.biombioe.2012.05.003

Yamatoya, K., Tabuchi, A., Suzuki, Y., & Yamada, H. (2020). Tamarind seed polysaccharide: Unique profile of properties and applications. *Biopolymer-based formulations*, 445–461.

Zhou, Y., Tang, S., Lv, Y., Zhang, D., Huang, X., Chen, Y., & Yong, Q. (2024). The prebiotic impacts of galactose side-chain of tamarind xyloglucan oligosaccharides on gut microbiota. *Heliyon, 10*(18). https://doi.org/10.1016/j.heliyon.2024.e37864